

# We are IntechOpen, the world's leading publisher of Open Access books Built by scientists, for scientists

6,900

Open access books available

186,000

International authors and editors

200M

Downloads

Our authors are among the

154

Countries delivered to

TOP 1%

most cited scientists

12.2%

Contributors from top 500 universities



WEB OF SCIENCE™

Selection of our books indexed in the Book Citation Index  
in Web of Science™ Core Collection (BKCI)

Interested in publishing with us?  
Contact [book.department@intechopen.com](mailto:book.department@intechopen.com)

Numbers displayed above are based on latest data collected.  
For more information visit [www.intechopen.com](http://www.intechopen.com)





supercapacitors: in series or parallel. For this last configuration, the two components are connected to the DC link through two choppers. In the series configuration (fig. 2), the supercapacitors is charged by the battery and discharged during the high power demand (startup, acceleration,...).

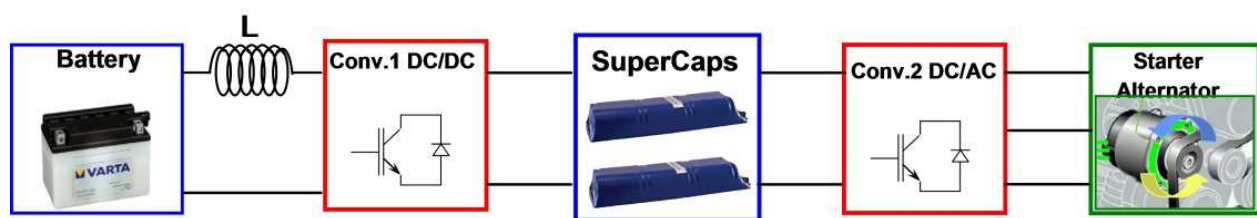


Fig. 2. Topology of the series hybrid supply for automotive application

Supercapacitors are chosen like booster because of their very high specific power, which can reach 17kw/kg. The capacitance of this component exceeds the 5000F (Maxwell technology) for a lower voltage (3V). To use this component in power applications, we must make some elements in series.



Fig. 3. Using the hybrid supply with starter or starter-alternator

### 3. Startup torque measurement

During the starting-up, the ICE develops a load torque applied to the starter or the starter-alternator. The computation of this torque allows us to validate the hybrid supply interest. To estimate this torque we need to know the evolution of the starter torque according to its current.

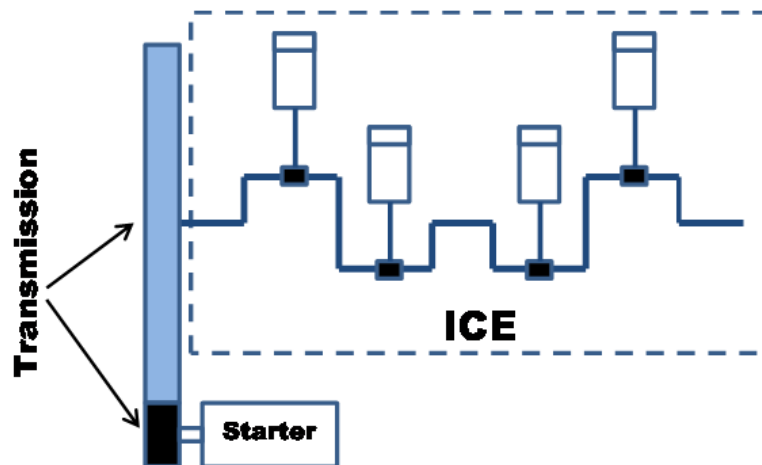


Fig. 4. The transmission between the starter and the ICE

### 3.1 Formula of the starter Torque

Because of their high starting torque, the series DC motors is used like a starter for the automobile applications. The torque developed by this motor can be written as follow:

$$T_{starter} = K \Phi I \quad (1)$$

The relation between the current and the flux of this type of motors complicates the identification of this torque. For that, this motor (starter) is transformed to a separate-wound DC motor.

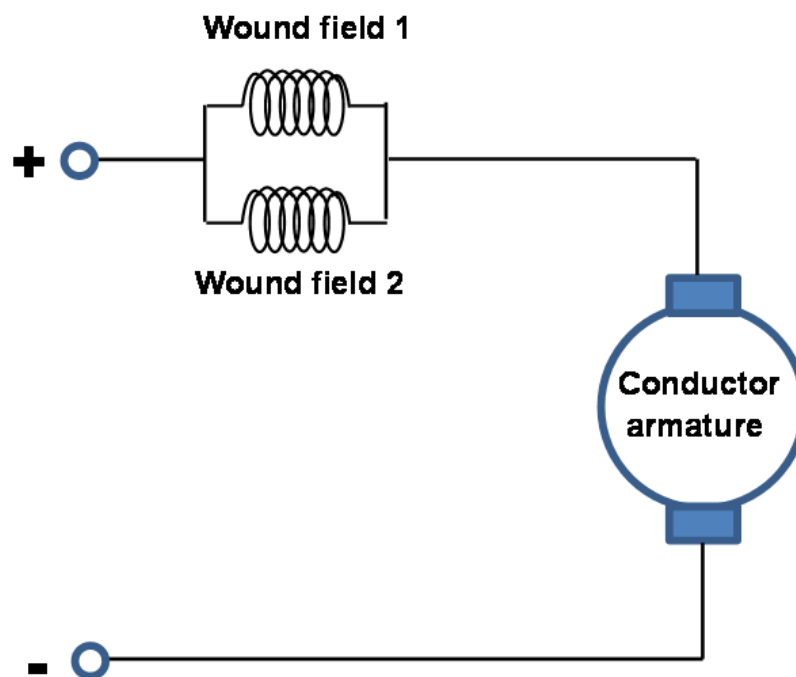


Fig. 5. Electrical diagram of starter (series motor).

Figure 6 presents the transformation of the series DC motor to a separate-wound DC motor. This transformation allows us to identify their torque.

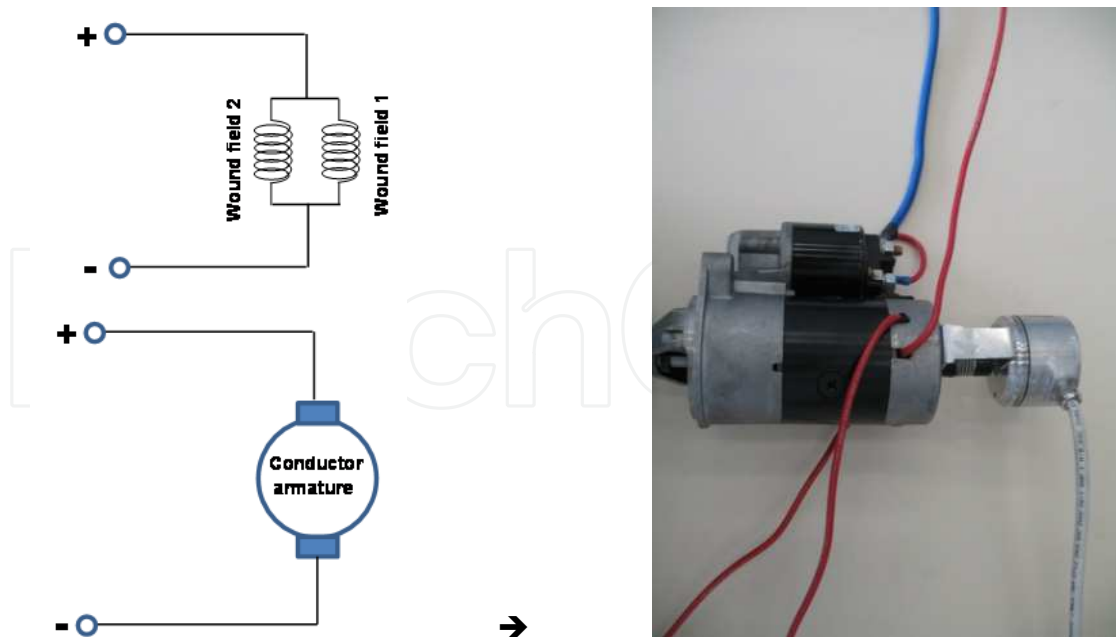


Fig. 6. Transformation of the series DC motor to separate-wound DC motor

The acquisition of the armature voltage, the armature current and the starter velocity at different wound current allows us to plot the evolution of the ratio  $K \Phi$  according to the current (fig. 7).

$$E = V - RI = K \Phi \Omega_{starter} \tag{2}$$

According to the results plotted on the figure 7, the ratio  $K \Phi$  can be written as follow:

$$K \Phi = -2 E - 9 I^3 + 3 E - 7 I^2 + 9 E - 5 I + 0,0063 \tag{3}$$

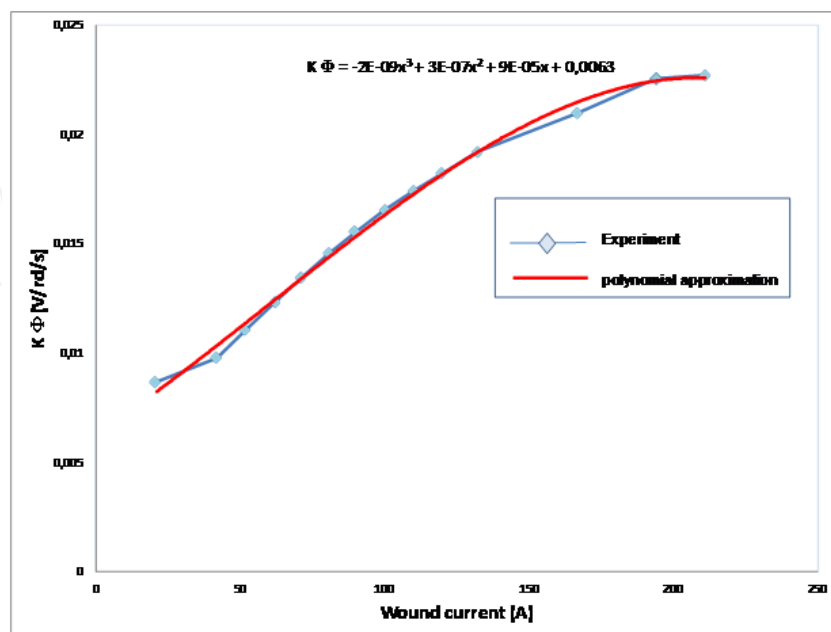


Fig. 7. Evolution of the ratio  $K \Phi$  according to the wound current

### 3.2 Formula of the startup torque

To identify the load torque developed by the ICE during the starting-up phase, two starting-up tests are made. The first it's without the spark plugs and the second it's with compression (with spark plug).

The first test (fig. 8) allows us to estimate the inertia and the friction torque of the ICE. Using the mechanic equation we can compute the two parameters ( $J$  and  $f$ ).

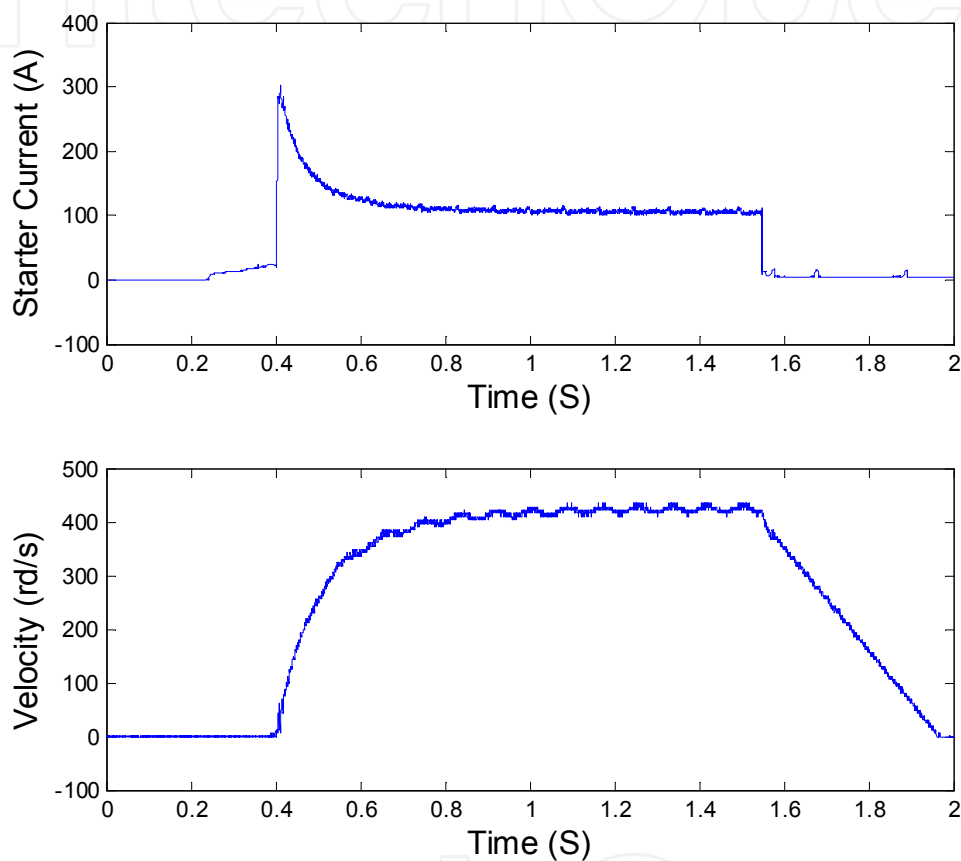


Fig. 8. Evolution of the current and the starter velocity for the test without spark plugs

$$J \frac{d\Omega}{dt} = K \Phi I - f \Omega - C_0 \quad (4)$$

Using the measured current and starter velocity, we can compute the parameters  $J$ ,  $f$  and  $C_0$ .

$$\begin{cases} J = 1.5 E - 3 \text{ Kg m}^2 \\ f = 4.2 E - 3 \text{ Nm / rd / s} \\ C_0 = 0 \text{ Nm} \end{cases} \quad (5)$$

The second test (fig. 9) allows us to estimate the rippled torque ( $T_{comp}$ ) due to the compression on the ICE motor.

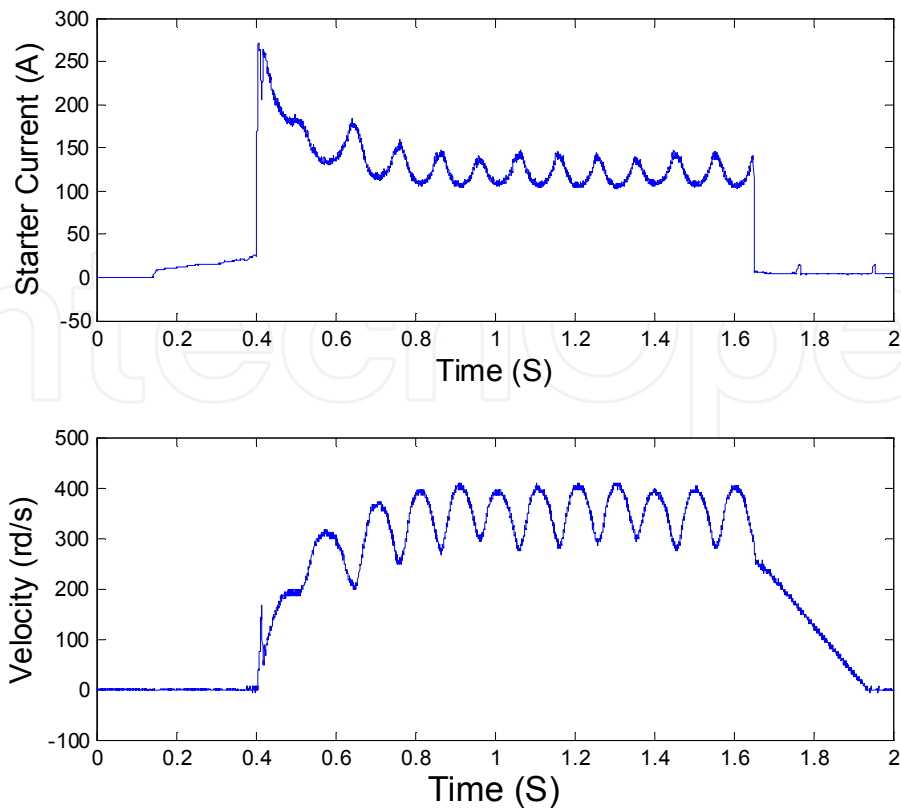


Fig. 9. Evolution of the current and the starter velocity for the test with spark plugs

Using the parameters computed at the first test ( $J$ ,  $f$  and  $C_0$ ), the current and the starter velocity presented in the figure 9, we can compute the torque due to the compression ( $T_{comp}$ ):

$$J \frac{d\Omega}{dt} = K \Phi I - f \Omega - C_0 - T_{comp} \quad (6)$$

Figure 10 presents the wave form of the compression torque  $T_{comp}$ . This can be written as:

$$T_{com} = 1 + 5.9 \sin(0.190 * \theta_{starter}) \quad (7)$$

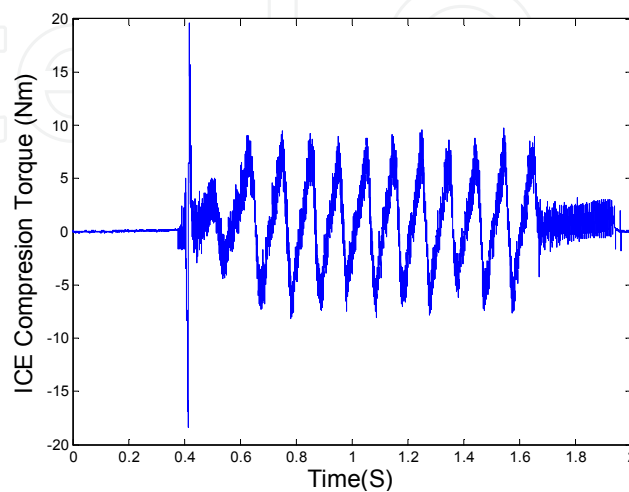


Fig. 10. Waveform of the compression torque  $T_{comp}$

#### 4. Sizing of the supercapacitors module for the startup

The supercapacitors sizing is based on the energy and power required for the starting-up of the vehicle. Figure 11 presents the evolution of the current and the voltage of the Buggy starter at the starting-up phase. At the beginning of this phase, the battery voltage decreases to reach 9V. At the same time, the current exceeds the 250A, what gives us a maximum power of 2400W.

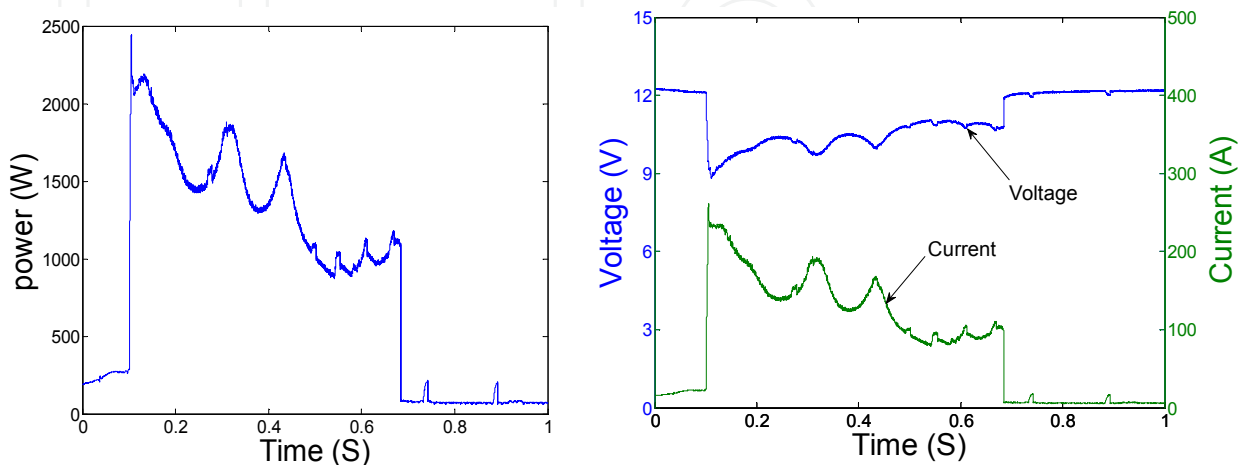


Fig. 11. Power and energy required for the starting-up of the vehicle

In order to ensure the functioning of the boost chopper, the minimum voltage of the supercondensator should not decrease lower than 12V (battery voltage). To take a safety margin, the minimum supercapacitors voltage is chosen about 15V. For this component, more than 75% of energy is stored between the maximum voltage of supercapacitors ( $V_{\max\_SupCaps}$ ) and the half of this voltage ( $V_{\max\_SupCaps}/2$ ):

$$V_{\min\_SuperCaps} = V_{\max\_SuperCaps} / 2 \Rightarrow V_{\max\_SuperCaps} = 2 V_{\min\_SuperCaps} = 30V \quad (8)$$

The power integral on all the starting-up duration allows us to compute the energy required for this phase.

$$E_{start} = \int P_{start} dt = 250mWh \quad (9)$$

The supercapacitors efficiency reaches 80% for 250A of RMS current.

By the neglecting of the Conv.2 losses, the starting-up energy can be written as follow:

$$E_{start} = \eta_{sc} \frac{1}{2} C_{sc} (V_{\max\_SuperCaps}^2 - V_{\min\_SuperCaps}^2) = \frac{3}{10} C_{sc} V_{\max\_SuperCaps}^2 \quad (10)$$

$$C_{sc} = \frac{10}{3} \frac{E_{start}}{V_{\max}^2} = \frac{10}{3} \frac{900}{30^2} \approx 3,34F \quad (11)$$

The best component for this application can be chosen using the characteristics of all Maxwell cells. The element 2,5V/310F gives us the best compromise between the power and the energy of the component.

	2.5V/4F	2.5V/10F	2.5V/120F	2.5V/140F	2.5V/310F	2.5V/350F	2.7V/650F	2.7V/1200	2.7V/1500	2.7V/2000	2.7V/3000
Tension (v)	2.5	2.5	2.5	2.5	2.5	2.5	2.7	2.7	2.7	2.7	2.7
Capacité d'un élément (F)	4	10	120	140	310	350	650	1200	1500	2000	3000
Courant (A)	1	8	2.5	19	730	530	1500	3500	3750	3900	4800
Nombre d'élément en série	11	11	11	11	12	12	12	12	12	12	12
Nombre de branches en parallèle	240	30	96	13	1	1	1	1	1	1	1
Capacité globale (F)	87.2727273	10.9090909	87.2727273	11.8181818	10	11.6666667	25.8333333	29.1666667	54.1666667	100	125
Volume unitaire (l)	0.0015	0.0015	0.003	0.003	0.027	0.027	0.053	0.053	0.211	0.294	0.373
Volume global (l)	3.96	0.495	3.168	0.429	0.324	0.324	0.636	0.636	2.532	3.528	4.476
Temps de charge à 20A	103.125	12.890625	103.125	13.964375	14.0625	16.40625	36.328125	41.015625	88.846875	164.025	205.03125
Resistance interne RMS (mOhm)	18.33333333	146.6666667	20.625	162.3076923	60	66.4	26.4	38.4	9.6	6.96	5.64

Table 1. Supercapacitors sizing

$$C_{component} = 310F; V_{component} = 2,5V;$$

$$N^{\circ}_{elements-en-series} = 12; N^{\circ}_{Branches} = 1 \tag{12}$$

$$Volume = 1l; RMS = 26m\Omega;$$

To reach 30V for the supercapacitors module, we must make 12 elements in series, what give a capacitance module about 26F:

$$C_{module} = \frac{310F}{12} = 26F \tag{13}$$

With this component, we can make 8 starting-up without reloading the component:

$$N_{start} = \frac{26F}{3,34F} \approx 8 \text{ starting-up} \tag{14}$$

### 5. Simulation of the system

Before the development of the test bench for this application, a simulation of the operated system is carried out using Matlab-Simulink software. In this case an inverter is used to

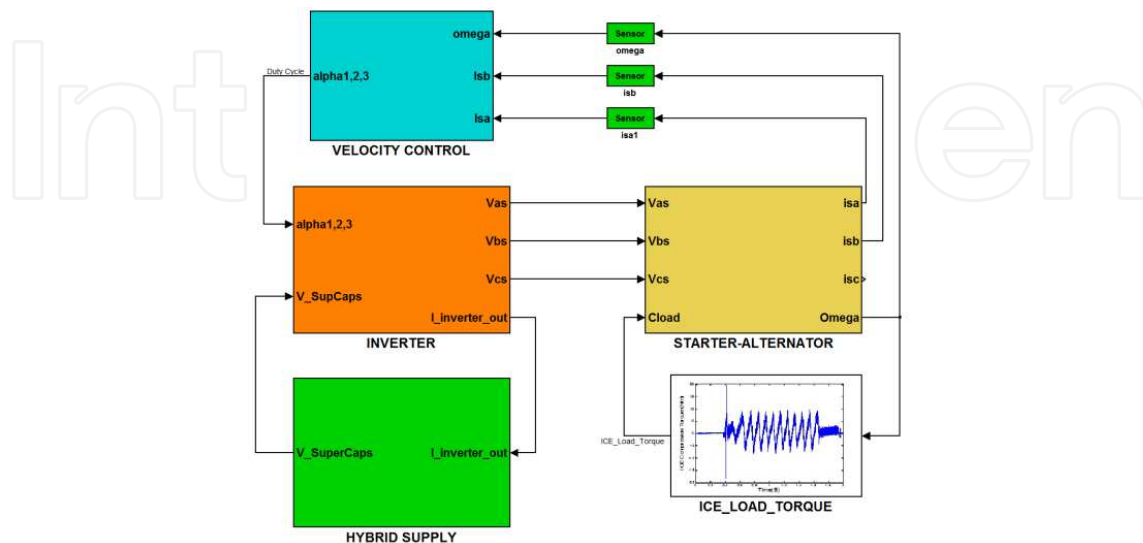


Fig. 12. Simulink model of the global system

supply the starter-alternator. In the startup phase, the velocity of the starter-alternator is controlled to reach the set point value (70 rd/S). The load torque is expressed according to the velocity using the formula 7.

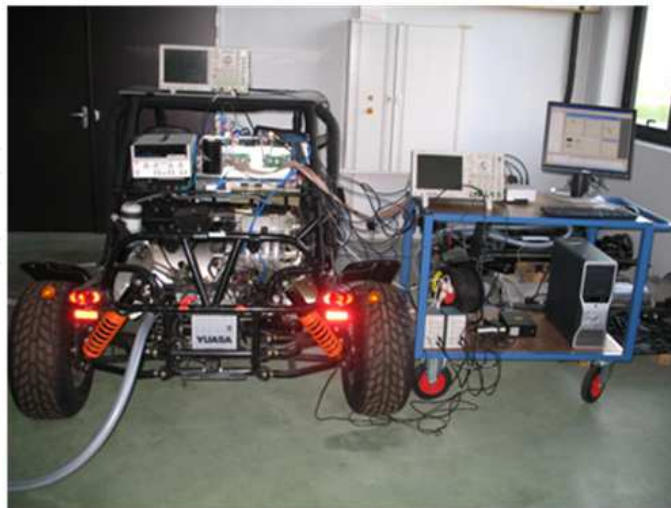


Fig. 13. Test bench developed on the mechatronic laboratory

To avoid the angular representation, the starter-alternator is modeled with two phases inputs/outputs (d,q). The model is transformed into three phases inputs/outputs using the Park's transformations. The rotoric current and the load torque generates by the ICE are considered also like inputs. The starter alternator equations can write as follow:

$$\begin{aligned}
 V_{sd} &= R_a i_{sd} + L_{sd} \frac{di_{sd}}{dt} - p L_{sq} i_{sq} \Omega \\
 V_{sq} &= R_a i_{sq} + L_{sq} \frac{di_{sq}}{dt} + p L_{sd} i_{sd} \Omega + k p M_{af} I_f \Omega \\
 C_{em} &= \frac{3}{2} p \left[ k M_{af} I_f I_{sq} + (L_{sd} - L_{sq}) I_{sd} I_{sq} \right]
 \end{aligned}
 \tag{15}$$

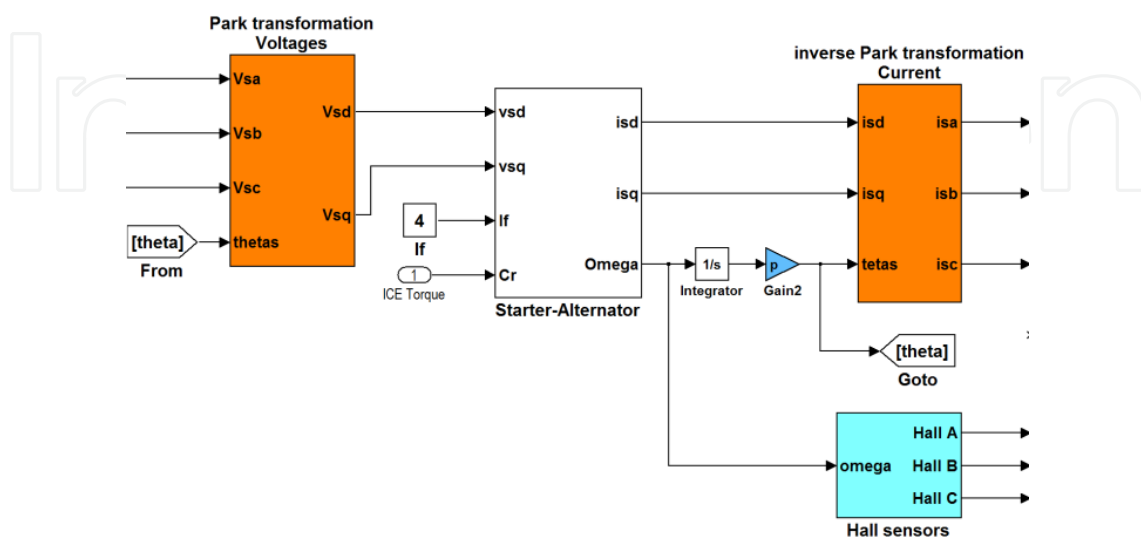


Fig. 14. Model of the starter-alternator

The starter-alternator parameters ( $L_{sd}$ ,  $L_{sq}$ ,  $R_a$ ,  $M_{af}$ ) are identified making some tests. The supplying of the two phases of the starter-alternator by two bridges chopper (fig. 15) at high frequency signal (20 kHz) allows to compute the values of the two inductances  $L_{sd}$  and  $L_{sq}$ . These last ones are computed for two positions of the rotor.

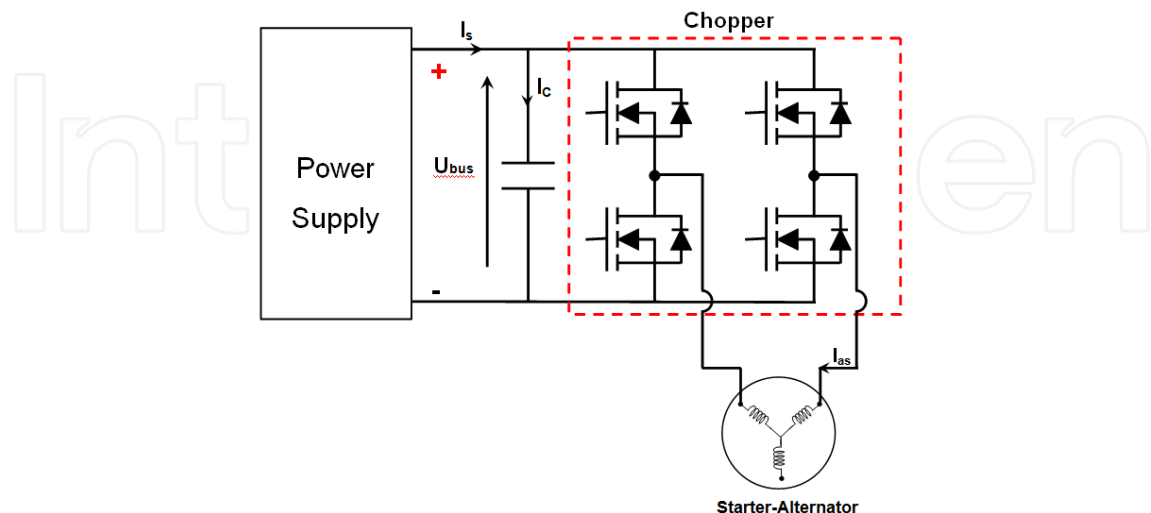


Fig. 15. Identification of the starter-alternator inductances

The first position (fig. 16.a) gives us the value of the direct inductance ( $L_{sd}$ ), and The second position of the rotor (fig. 16.b) gives us the value of the quadratic inductance ( $L_{sq}$ ). The same formula is used to calculate the two inductances:

$$\begin{cases} L_{sx} = U_{bus} \frac{\Delta t}{2 \Delta i} \\ x = d \text{ or } q \end{cases} \quad (16)$$

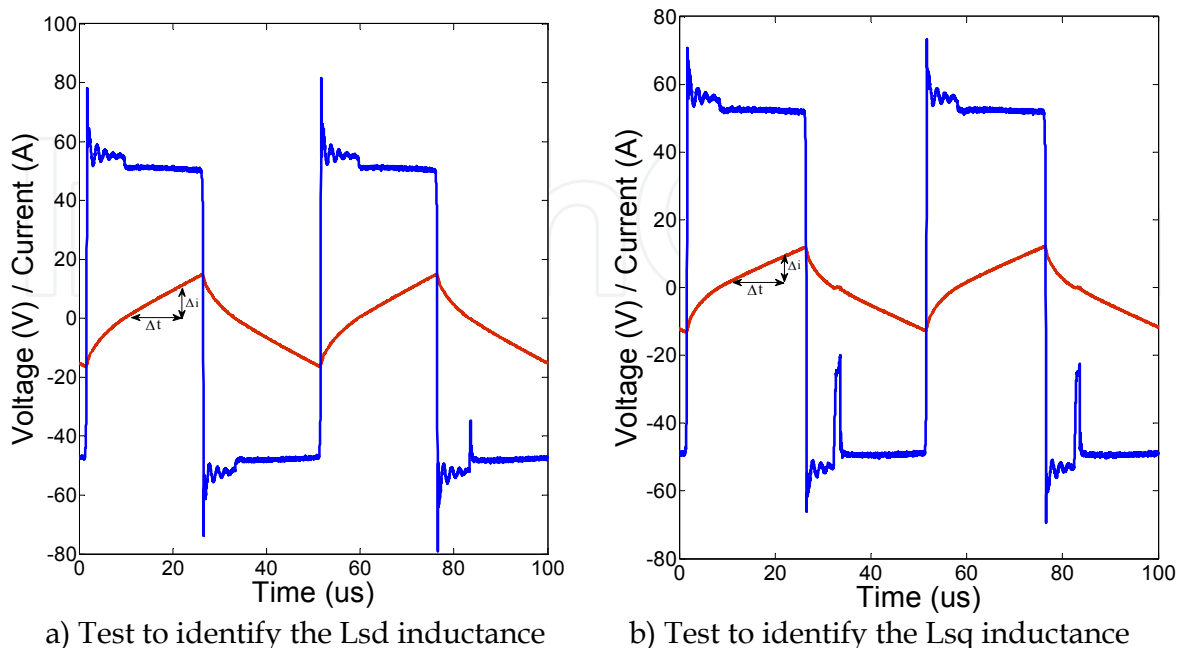


Fig. 16. Identification of the machine inductances

The applying of this formula gives us the values of Lsd and Lsq:

$$\begin{cases} L_{sd} = 40,7 \mu H \\ L_{sq} = 28 \mu H \end{cases} \quad (17)$$

To calculate the parameter Maf, the starter alternator must turn at constant velocity with the variation of the inductor current. In this case, the value of the voltage between two phases can expressed as follow:

$$\frac{U_{ab}}{\sqrt{3}} = \frac{p M_{af} I_f \Omega}{\sqrt{2}} \Rightarrow M_{af} = \frac{\sqrt{2}}{\sqrt{3}} \frac{U_{ab}}{2 \pi f p I_f} \quad (18)$$

Table 2 summarizes the values of the starter-alternator parameters:

Parameter	Value	unit
Lsd	40	$\mu H$
Lsq	40	$\mu H$
Ra	13.3	m $\Omega$
Maf	2.5	mH

Table 2. Starter alternator parameters

The inverter is modeled using the formulas between the starter-alternator voltages ( $V_{as}, V_{bs}$  and  $V_{cs}$ ) and the control of the semiconductors ( $K_1, K_2$  and  $K_3$ ):

$$\begin{bmatrix} V_{as} \\ V_{bs} \\ V_{cs} \end{bmatrix} = \frac{U_{bus}}{3} \cdot \begin{bmatrix} 2 & -1 & -1 \\ -1 & 2 & -1 \\ -1 & -1 & 2 \end{bmatrix} \cdot \begin{bmatrix} K_1 \\ K_2 \\ K_3 \end{bmatrix} \quad (19)$$

The voltage of the Dc link is also one of the inputs for the inverter model. On the other hand, this model imposes the current of the hybrid supply. This last one is composed with two storage systems (battery and supercapacitors) associated with a chopper (fig. 17), which is connected to the battery through an inductive filter.

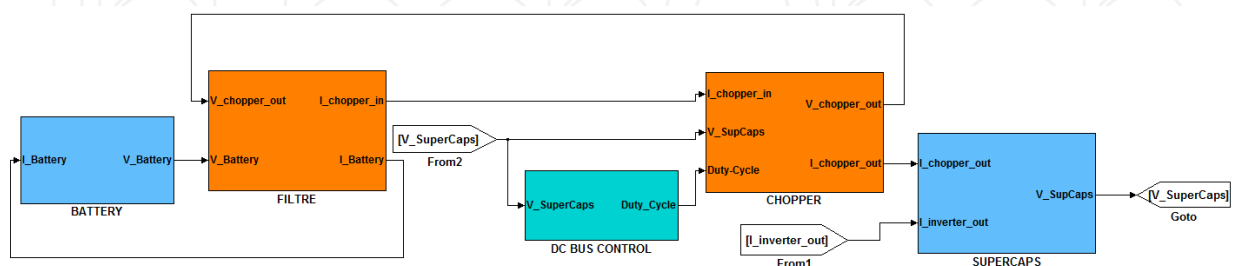


Fig. 17. Simulink model of the hybrid supply

Two models are used to represent the battery behaviour. The first one is the simplified R-C model which uses just a resistance and capacitance to modelling the battery. The second representation is based on the frequency behaviour of the battery. This method allows the representation of the component using the Shepherd model (fig. 18)

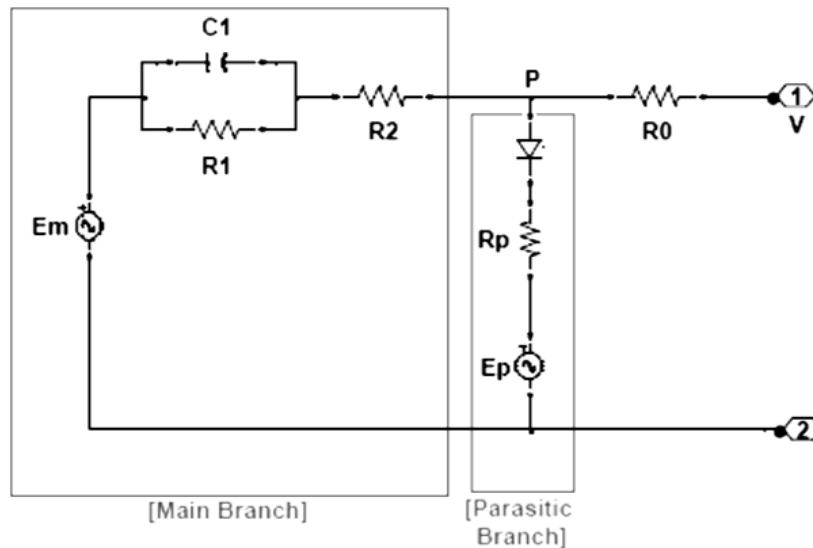


Fig. 18. Shepherd model of the battery

For the supercapacitors modeling a transmission line model is used. This approach is based on the representation of the charges propagation along the electrodes surface by RC circuits. So, the supercapacitor is considered like a capacitance distributed along the volume, with accessible areas and less accessible ones. The distribution of the capacitance depends on the electrode material and especially on the geometrical properties of the pores where ions have to access to constitute the double layer capacitance. This approach is well represented by an electrical circuit representing the transmission line and using r-c parallels branches. Then, the proposed model will only include 3 parameters ( $C$ ,  $r_s$  and  $R$ ).

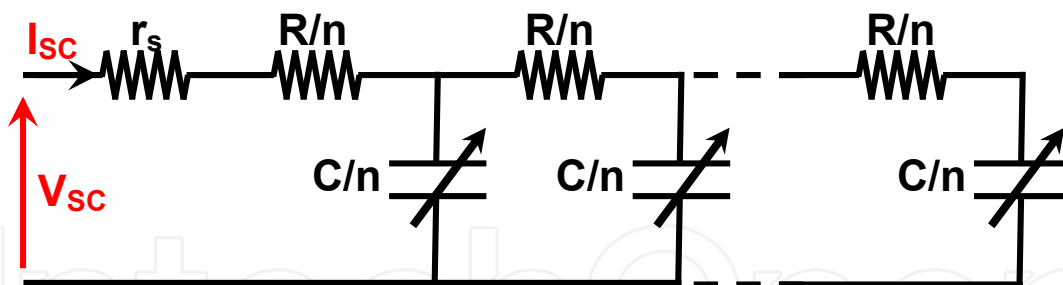


Fig. 19. Transmission line model

The modelling of the chopper is made making the formulas between the inputs and outputs of this converter (fig. 20).

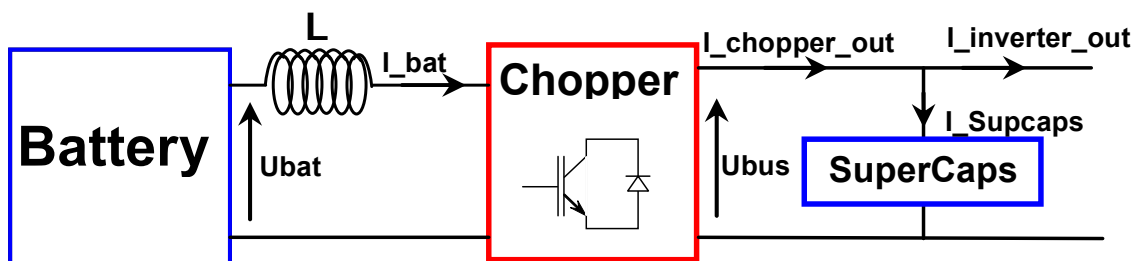


Fig. 20. Chopper inputs/outputs

The relations between the inputs and outputs of the chopper can write as follow:

$$\begin{cases} I_{bat} = \left[ (U_{bat} - ((1 - \alpha)U_{bus})) \right] \frac{1}{Ls} \\ I_{chopper\_out} = (1 - \alpha)U_{bus} I_{bat} \\ I_{SupCaps} = I_{inverter\_out} - I_{chopper\_out} \end{cases} \quad (20)$$

The starter-alternator velocity is estimated through Hall sensors. Using the three phases positions (fig. 21), given by these sensors we can estimate the velocity and the electric angle of the starter-alternator

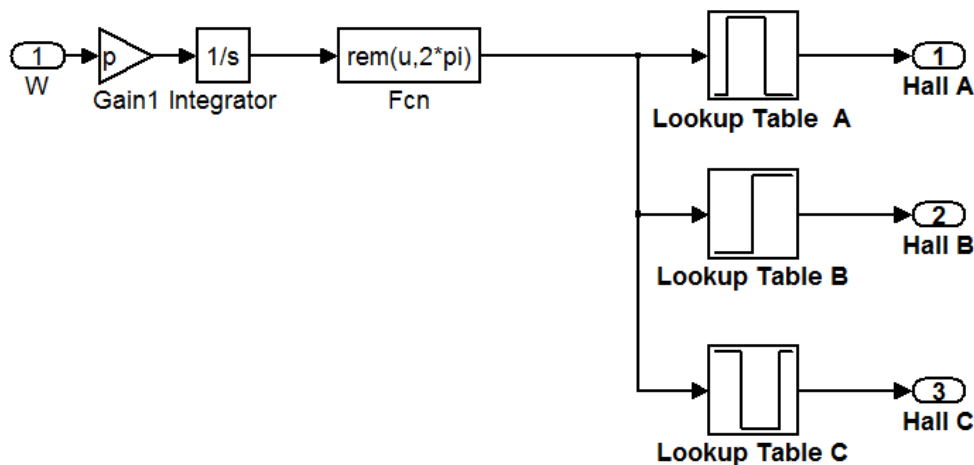


Fig. 21. Starter-alternator position using Hall sensor

## 6. Simulation results

Two simulations of the system functioning are made using the developed model. The first model it's to validate the startup of the vehicle using the hybrid supply. In this case, the supercapacitor discharge and the voltage of the DC link decreases. The second test is to validate the electric power generation and the charge of the battery.

### 6.1 Startup of the vehicle using the hybrid supply

To turn-on the vehicle, the velocity of the starter-alternator is controlled to reach the set point value (32rd/s). During this phase, the supercapacitor discharge. Figure 22 presents the waveform of the starter-alternat or velocity (real velocity) and that estimated using the hall sensors. This figure shows also that the starter-alternator velocity reaches the set-point value after 50 ms.

Figure 23 presents the waveform of the electric angle and that estimated using the hall signals. This result shows the deference between the real value of the electric angle and that estimated for the low velocity. After that the estimation gives almost the real value.

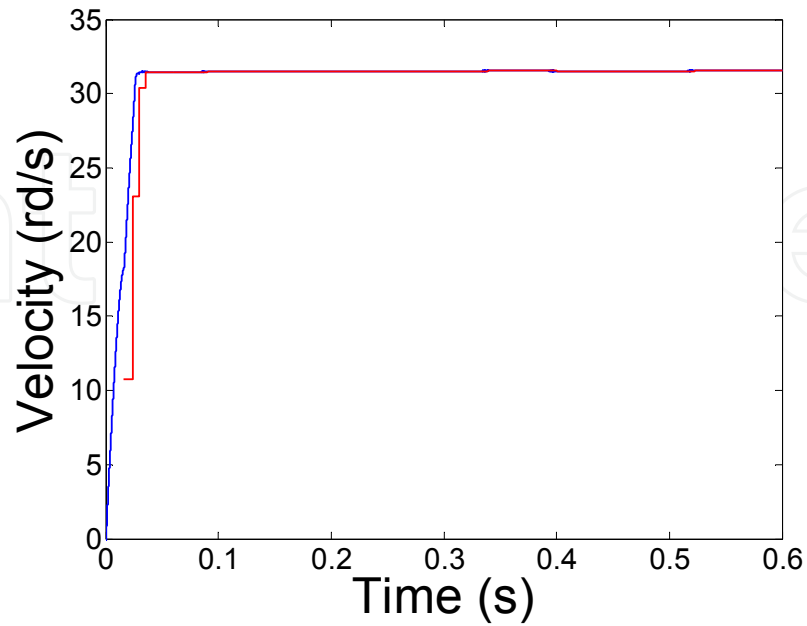


Fig. 22. Velocity of the starter-alternator during the start-up phase

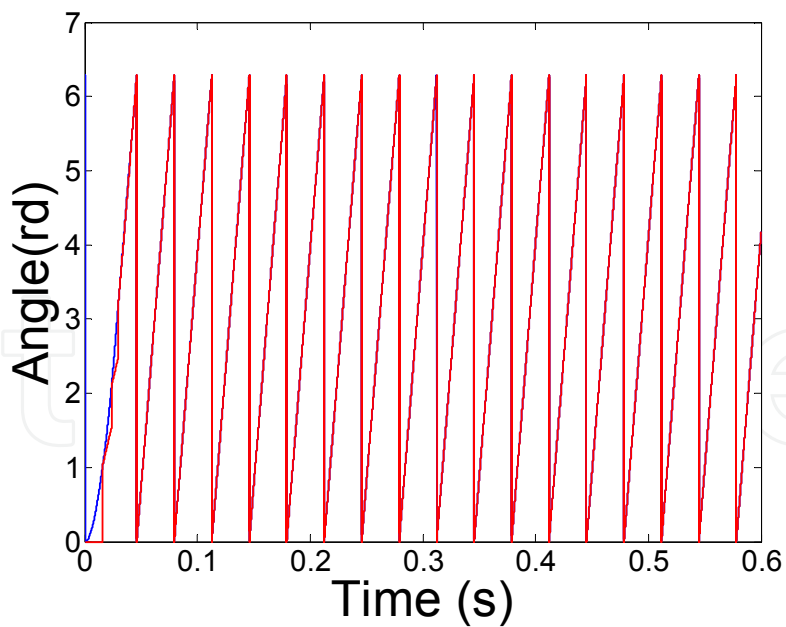


Fig. 23. Angle of the starter-alternator during the start-up phase

Figure 24 presents the evolution of starter-alternator current during the startup phase. This result shows that the current for the startup phase reach 560A at the beginning and stabilize after that at 280A.

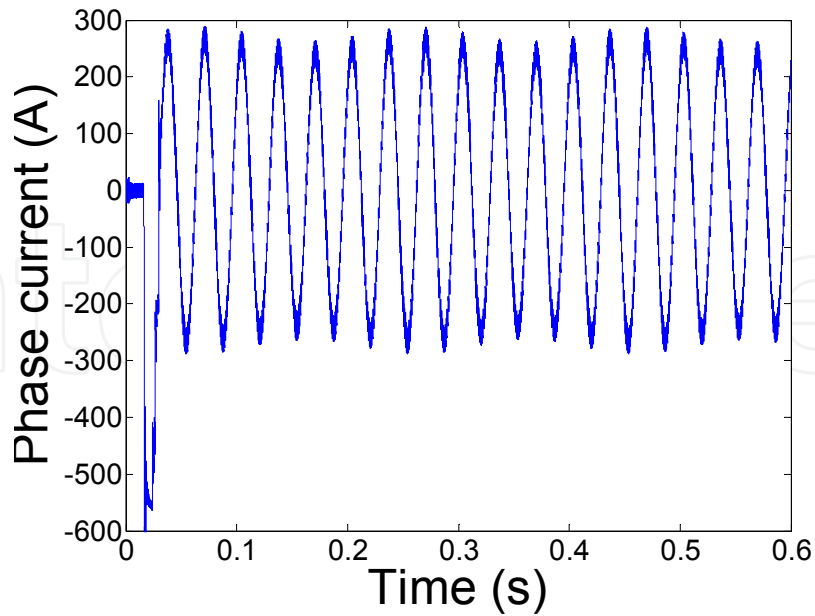


Fig. 24. Current of the starter-alternator during the start-up phase

During the startup phase, the supercapacitors current reaches -90A at the beginning and stabilizes after that at -38A. In this case, the supercapacitors discharge and the voltage of this component decreases. During this phase, the battery charges the supercapacitors at low current (20A) and the SOC of this component decreases from 100% to 99.8%.

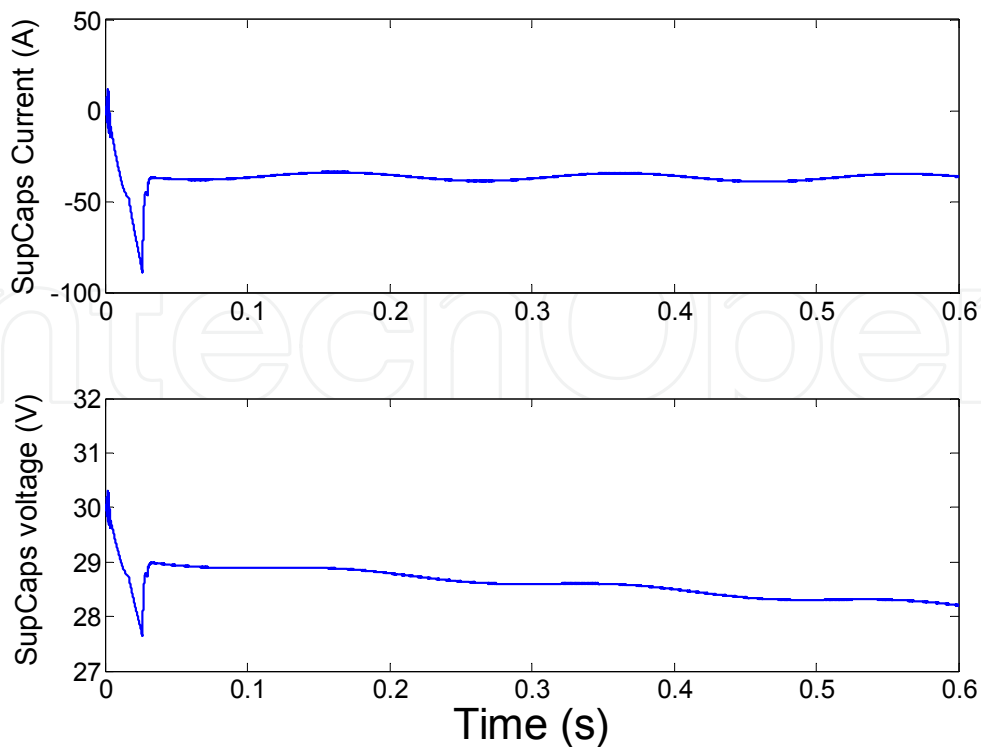


Fig. 25. Current and voltage of the supercapacitor module during the start-up phase

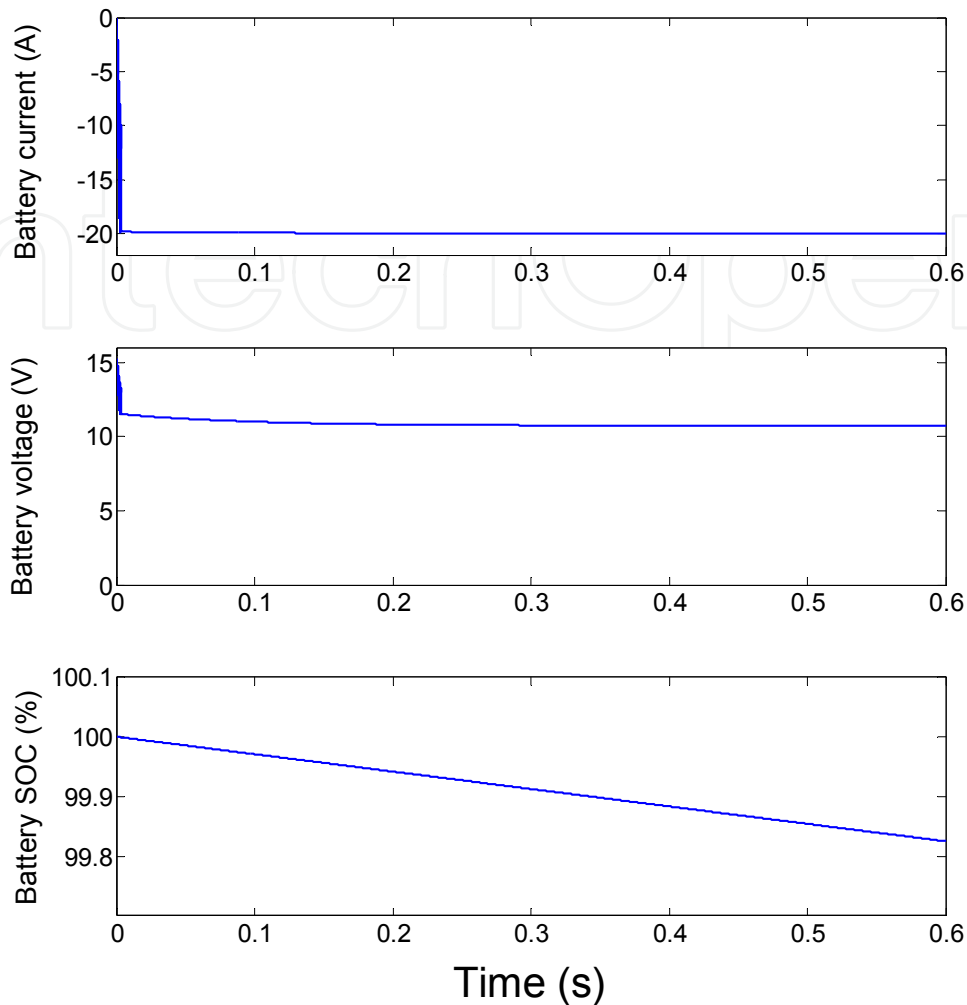


Fig. 26. Current, voltage and SOC of the battery during the start-up phase

## 6.2 Electric power generation

When the engine is turned-on, the starter alternator charges the battery and the supercapacitors. Firstly, the supercapacitors is charged with high current to reach 30V (fig. 27). In the same time, the chopper insures the charge of the battery. In this case, the voltage of the battery is controlled to reach the set point value (13V). During this time, the state of charge increases (fig. 28).

The battery current is limited between -20A and +20A. At the beginning, the battery participate to charge the supercapacitor module and after that the battery current reaches 20A, in the same time battery SOC increases during this phase.

The ICE drive the starter-alternator and this last one provide the power needed to charge the battery (fig. 28 and 29). The current in this case is very low compared to that of the startup phase (280A for the sturtup and 4A to charge the battery).

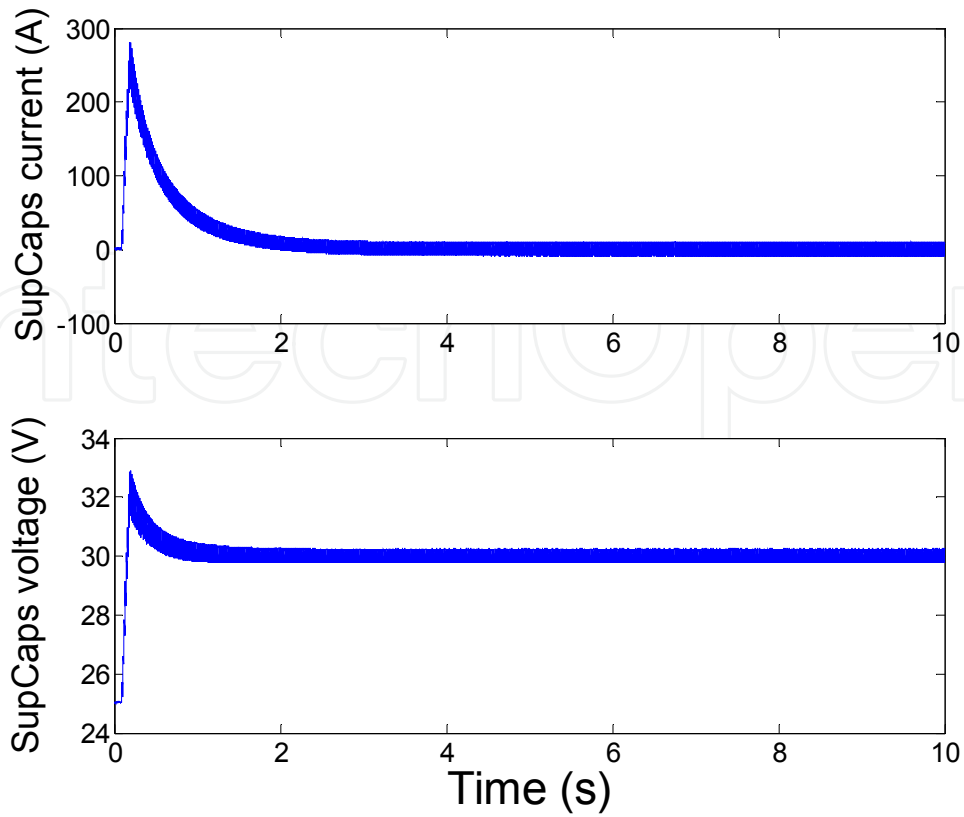


Fig. 27. Current and voltage of the supercapacitor module during the power generation phase

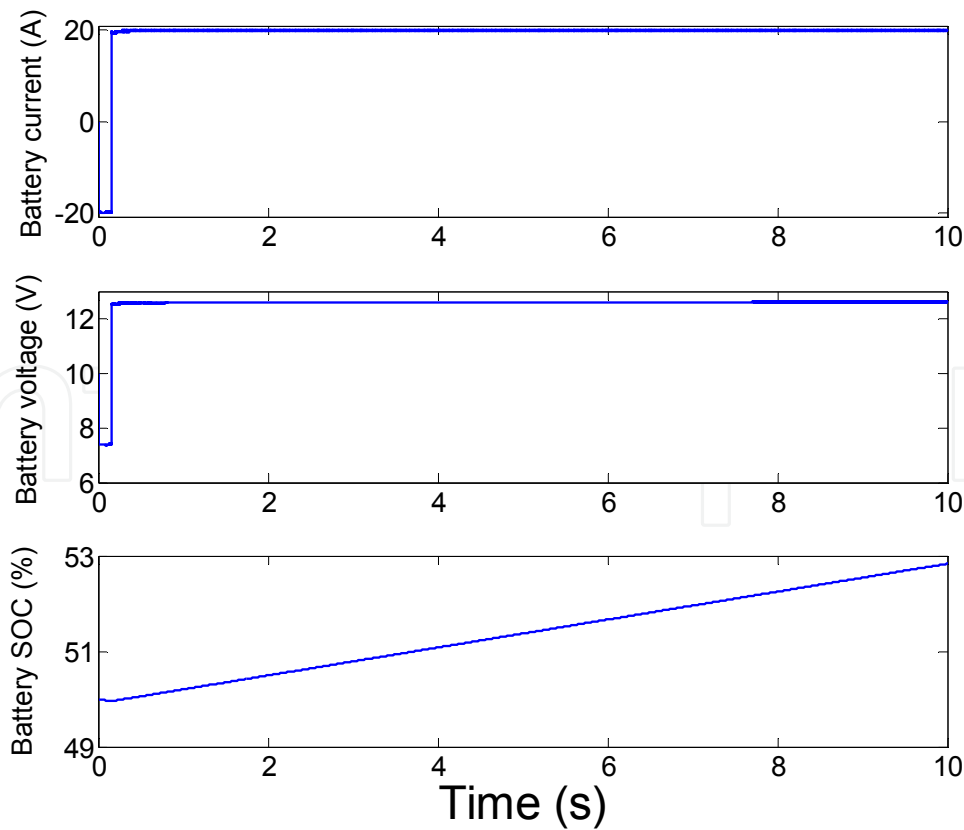


Fig. 28. Current, voltage and SOC of the battery during the power generation phase

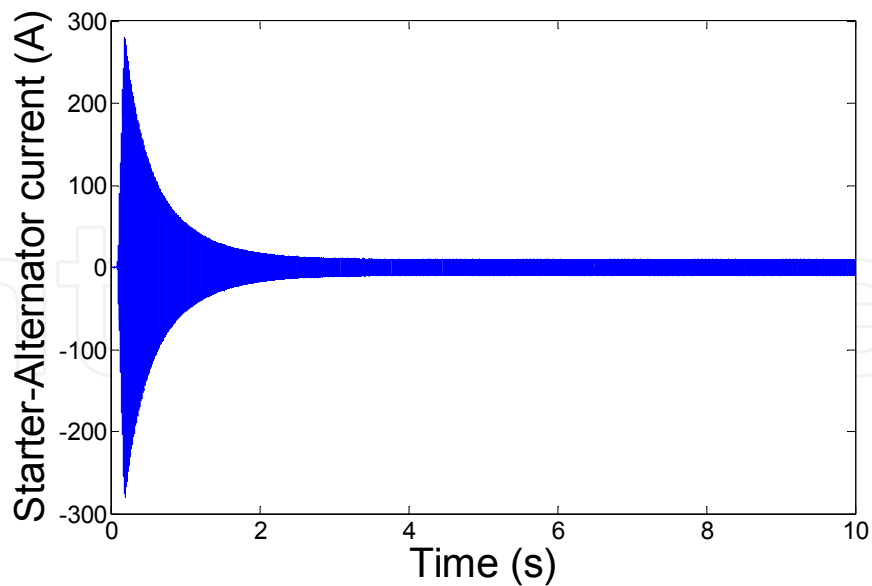


Fig. 29. Waveform of the phase current during the power generation phase (during 2 seconds)

In the power generation phase, the inverter is used like a synchronous rectifier and the signal period depends to the engine velocity.

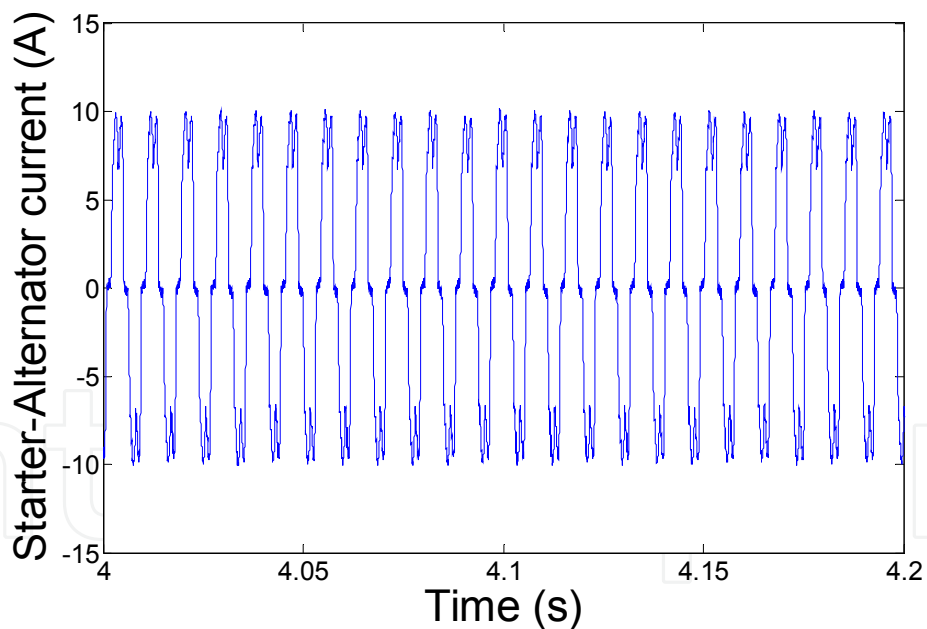


Fig. 30. Waveform of the current during the power generation phase (during 0.2 seconds )

## 7. Conclusion

The batteries used for the micro-hybrid vehicles have very high specific energy. Unfortunately, the power of this technology is very low compared to other technologies (Ni-Mh, Li-Ion,...). The association of battery for this application (micro-hybrid) with powerful component like supercapacitors can decrease the weight of the battery and/or ameliorate

the lifetime of the supply. In this paper, hybrid supply for micro-hybrid vehicle has been presented. In this case, two storage components are used: supercapacitors like power supply and battery like energy supply. The power density of supercapacitors makes them very interesting for the applications which need high power during short time.

Two architectures are possible to implement the association of supercapacitors and battery: a parallel architecture by connecting the two sources to DC bus through two choppers. The drawback of this architecture is the very large size of the induction coil in series with the supercapacitor module. In the case of series architecture, the size of the induction coil used to smooth the battery current is less important because of the weakness of the current charge/discharge.

After the choose of the architecture of the power supply and the identification of the load torque, the parameters of the starter-alternator are identified. In the next part, the sizing of the two storage system (battery and supercapacitors) is presented.

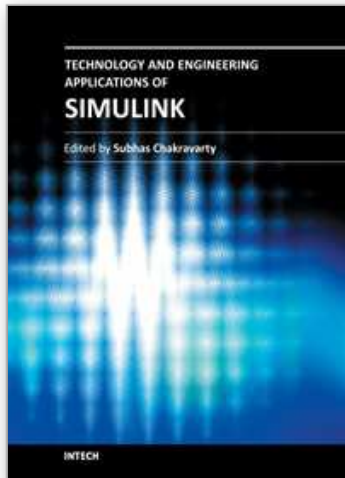
Matlab-simulink software is used to simulate the supplying of the starter-alternator by the hybrid supply through an inverter. The association of battery and supercapacitors is made using a boost chopper. For the startup phase, the velocity of the starter-alternator is controlled to follow the set point value (32rd/s).

## 8. References

- N. Rizoug (2006), *Modélisation électrique et énergétique des supercondensateurs et méthodes de caractérisation : Application au cyclage d'un module de supercondensateurs basse tension en grande puissance*, Thesis, feb 2006, Ecole centrale de Lille.
- P. Bartholomeüs, B. Vulturescu, X. Pierre, N. Rizoug, P. Le Moigne (2001), *A 60V-400A test bench for supercapacitor modules*, EPE'2003, Toulouse, Septembre 2003.
- S. Buller, E. Karden, D. Kok, R.W. De Doncker (2001), *Simulation Of Supercapacitors In Highly Dynamic Applications*, ESV, 2001, Berlin, Germany.
- N. Rizoug, P. Bartholomeüs, P. Le Moigne and B. Vulturescu (2004), *Electrical and thermal behaviour of a supercapacitor module: on-line characterization*, ESSCAP'2004, Belfort, France.
- Y. Hyunjae, S. Seung-Ki, P. Yongho and J. Jongchan (2007), *System Integration and Power-Flow Management for a Series Hybrid Electric Vehicle Using Supercapacitors and Batteries*, IEEE Trans. Ind. Applic, Vol. 44, N° 1, pp. 108-114, Jan.-feb. 2007.
- C. Plasse, A. Akémakou, P. Armioli and D. Seville (2003), *L'alternateur-Demarreur, Du Stop And Go Au Groupe Motopropulseur Mild Hybride*, Prop'Elec 2003, France 2003.
- J.M. Dubus, P. Masson and C. Plasse (2003), *The Starter Alternator Reversible Systems Of Valeo*, Valeo Systèmes Electriques.
- S. B. Ozzturk, B. Akin, H. A. Toliyat and F. Ashrafzadeh (2006), *Low-Cost Direct Torque control of Permanent Magnet Synchronous motor using Hall-effect sensors*, IEEE APEC 2006.
- D. Feroldi, M. Serra and J. Riera (2009), *Design and Analysis of Fuel-Cell Hybrid Systems Oriented to Automotive Applications*, IEEE Trans. Veh. Technol., vol. 58, no. 9, Nov. 2009.
- W. Gao (2005), *Performance Comparison of a Fuel Cell-Battery Hybrid Powertrain and a Fuel Cell-Ultracapacitor Hybrid Powertrain*, IEEE Trans. Veh. Technol., vol. 54, no. 3, May 2005.

- J. Bauman and M. Kazerani (2008), *A Comparative Study of Fuel-Cell-Battery, Fuel-Cell-Ultracapacitor, and Fuel-Cell-Battery-Ultracapacitor Vehicles*, IEEE Trans. Veh. Technol., vol. 57, no. 2, Mar. 2008.
- S. Lu, Keith A. Corzine and M. Ferdowsi (2007), *A Unique Ultracapacitor Direct Integration Scheme in Multilevel Motor Drives for Large Vehicle Propulsion*, IEEE Trans. Veh. Technol., vol. 56, no. 4, JULY 2007.
- Y. Yang, J. Liu, T. Wang, K. Kuo and P. Hsu (2007), *An Electric Gearshift With Ultracapacitors for the Power Train of an Electric Vehicle With a Directly Driven Wheel Motor*, IEEE Trans. Veh. Technol., vol. 56, no. 5, Sep. 2007.

IntechOpen



## **Technology and Engineering Applications of Simulink**

Edited by Prof. Subhas Chakravarty

ISBN 978-953-51-0635-7

Hard cover, 256 pages

**Publisher** InTech

**Published online** 23, May, 2012

**Published in print edition** May, 2012

Building on MATLAB (the language of technical computing), Simulink provides a platform for engineers to plan, model, design, simulate, test and implement complex electromechanical, dynamic control, signal processing and communication systems. Simulink-Matlab combination is very useful for developing algorithms, GUI assisted creation of block diagrams and realisation of interactive simulation based designs. The eleven chapters of the book demonstrate the power and capabilities of Simulink to solve engineering problems with varied degree of complexity in the virtual environment.

### **How to reference**

In order to correctly reference this scholarly work, feel free to copy and paste the following:

N. Rizoug, G. Feld, B. Barbedette and R. Sadoun (2012). Using of Hybrid Supply for Electric or Hybrid Vehicles, Technology and Engineering Applications of Simulink, Prof. Subhas Chakravarty (Ed.), ISBN: 978-953-51-0635-7, InTech, Available from: <http://www.intechopen.com/books/technology-and-engineering-applications-of-simulink/using-of-hybrid-supply-to-supply-electric-or-hybrid-vehicles>

# **INTECH**

open science | open minds

### **InTech Europe**

University Campus STeP Ri  
Slavka Krautzeka 83/A  
51000 Rijeka, Croatia  
Phone: +385 (51) 770 447  
Fax: +385 (51) 686 166  
[www.intechopen.com](http://www.intechopen.com)

### **InTech China**

Unit 405, Office Block, Hotel Equatorial Shanghai  
No.65, Yan An Road (West), Shanghai, 200040, China  
中国上海市延安西路65号上海国际贵都大饭店办公楼405单元  
Phone: +86-21-62489820  
Fax: +86-21-62489821

© 2012 The Author(s). Licensee IntechOpen. This is an open access article distributed under the terms of the [Creative Commons Attribution 3.0 License](#), which permits unrestricted use, distribution, and reproduction in any medium, provided the original work is properly cited.

IntechOpen

IntechOpen